Passivity and Stability of Human–Robot Interaction Control for Upper-Limb Rehabilitation Robots

Juanjuan Zhang and Chien Chern Cheah

Abstract—Each year, stroke and traumatic brain injury leave millions of survivors with motion control loss, which results in great demand for recovery training. The great labor intensity in traditional human-based therapies has recently boosted the research on rehabilitation robotics. Existing controllers for rehabilitative robotics cannot solve the closed-loop system stability with uncertain nonlinear dynamics and conflicting human–robot interactions. This paper presents a theoretical framework that establishes the passivity of the closed-loop upper-limb rehabilitative robotic systems and allows rigorous stability analysis of human–robot interaction. Position-dependent stiffness and position-dependent desired trajectory are employed to resolve the possible conflicts in motions between patient and robot. The proposed method also realizes the "assist-as-needed" strategy. In addition, it handles human–robot interactions in such a way that correct movements are encouraged and incorrect ones are suppressed to make the training process more effective. While guaranteeing these properties, the proposed controller allows parameter adjustment to provide flexibility for therapists to adjust and fine tune depending on the conditions of the patients and the progress of their recovery. Simulation and experiment results are presented to illustrate the performance of the method.

Index Terms—Adaptive control, human–robot interaction, rehabilitation robotics.

I. INTRODUCTION

NEURAL damages in the form of stroke or traumatic brain injuries produce millions of new patients of paralysis each year, which creates great need of therapeutic training for lost or impaired motion control restoration. The theory of synaptic plasticity [1], which was later summarized as "neurons that fire together, wire together" [2] has been proposed for more than a century. According to this principle, simultaneous activation of neurons leads to increase in synaptic strength between them and, therefore, relearning of human movements through "reconnection" of broken neurological path [3] in case of broken-neurological-path-paralysis or "reorganization" of brain [4] in case of damaged-brain-motor-cortex-paralysis. Therefore, repeated and concurrent happening of human intentions to move and limb movements is the key to recovery. Clinical one-on-one rehabilitative therapies have been introduced from the 1950s

to realize this process. However, traditional human-based practice is inefficient due to its great labor intensity [5] and bad repeatability. It totally relies on therapy and evaluation process conducted by one therapist attending one single patient at a time. Besides, the duration and frequency of these therapies are limited by the strength of practitioners. Lab-intensive activities stand for one key application area for robotics. To overcome the limitations of human-based practice, research on *rehabilitative robotics* has started since early 1990s, among which the MIT-MANUS upper-limb therapeutic training robot was a pioneer [6].

Robot systems can be classified into two general groups, *isolated* robotics that have no environmental contacts other than base support and *nonisolated* systems, which interact with the environment besides the base support, such as rehabilitation robotics. Control theories for the former with systematic stability analysis have already been established in the literature [7]–[10]. Control of rehabilitative systems, on the contrary, is different from the traditional robotic control in the sense that it is not always a servo mechanism [11]. Besides stability, there are two main objectives of a rehabilitative controller according to the training principle: encouraging human intentions to move and ensuring correct human movements. At an early stage, patients are either fully paralyzed or generating untrustworthy signals, the training should be *robot assisting*, i.e., rehabilitative robots work just like the assistive ones by treating all signals and interactions from the human as disturbances and traditional control methods are applicable. However, when motion-related neurological connection is restored but weak, the training should be *robot-complementing*, i.e., human intentions and movements should be encouraged and complemented rather than rejected [11]. In this case, traditional control methods are not suitable.

The primary control paradigm in robotic therapy development is the active assist exercise [12] that emulates physician-based therapies. In this type of controller, a human patient initiates a movement, or a predetermined desired trajectory is known to the robotic device. Then, the device will assist the user to move the limbs and fulfill the task. Existing assistive controllers of rehabilitative systems are mostly directly or indirectly derived from motion and impedance manipulation [13]. Some are model-based controllers with force feedback [14], [15] or without force feedback [11]. Others are model-free methods with less predictable real-time interactions between patients and devices and, thus, less control of the training progress [16]. More early devices employ motion-only-based control and handle interactions by disturbance rejection or uncertain modeling. This method is proper at the early stage of therapy for some severely paralyzed patients when functionality loss is almost total and patients' ability to move their limbs can be ignored. Among these controllers, simple PD control [5], [14] started with a dominant role. Later devices, for both upper limb [17] and lower limb [18], use similar strategy, but instead of asserting torques linearly related to position errors, more sophisticated force fields

are used to build a virtual moving wall in space along the desired trajectory. This demonstrates one form of the "assist-as-needed" paradigm, which is proved to be more effective in [19].

However, in these existing designs, stability of the systems is not systematically solved with nonlinearity, uncertainty, changing human dynamics or interaction forces [20], [21]. Besides, due to the fact that rehabilitative robotics work in close contact with impaired human, safety is a critical concern during the operation. Various causes can incur injuries to human in interaction with a robot [22] when the robot velocity, acceleration, or torque exceeds certain values. Possible injuries include bone damage, joint damage, and soft tissue fracture, severity of which may range from minor to fatal [22]. The situation is especially serious in case when robots work with motion-control-challenged human as in rehabilitation applications, when paralysis or spasticity causes high stiffness of human joint and inability to react fast. To maintain human safety throughout the operation, stability of the control systems must be ensured. Furthermore, the conflicting movements between human and robot should also be resolved in a stable manner to avoid large control forces and instability.

This paper proposes an adaptive control framework for the upper-limb rehabilitative robotic systems that can easily realize training decisions made by therapists. The proposed method handles human–robot interaction in such a way that "correct" human movements are encouraged while incorrect movements are compensated to ensure the efficiency of the training process. Position-dependent stiffness and desired trajectory are proposed to resolve the possible conflicts in motions between patients and robots. The main contributions of this paper include: 1) A theoretical framework which establishes system passivity and allows rigorous stability analysis of human–robot interaction in rehabilitative robotic system is presented. 2) The assist-as-needed policy is realized, while allowing customization of the controller based on different patients and their different stages to cope with the patient cooperative training [23]. 3) The conflicting movements between human and robot are reduced and contained in a stable manner to align with rehabilitation philosophy. A preliminary version of this paper was presented in ICRA2013 [24]. This paper is an extended version with more details in the theoretical analysis, formal statements of theorems, and new experimental results.

II. UPPER-LIMB REHABILITATIVE ROBOTICS DYNAMICS

The dynamics of an upper-limb rehabilitative robotic system consisting of a n-DOF robot manipulator connected to a human arm at the end can be expressed as

$$M(q)\ddot{q} + \left[\frac{1}{2}\dot{M}(q) + S(q,\dot{q}) \right] \dot{q} + g(q) = \tau + J^{\mathsf{T}}(q)f_h \quad (1)$$

where $q \in \Re^n$ is the joint displacement vector and $\dot{q} = \frac{dq}{dt} \in \Re^n$ is the joint velocity vector; $M(q) \in \Re^{n \times n}$ is the manipulator inertia matrix, which is symmetric and positive definite; $[\frac{1}{2}\dot{M}(q) + S(q,\dot{q})]\dot{q} \in \Re^n$ is the centripetal and Coriolis torques, in which $S(q,\dot{q}) \in \Re^{n \times n}$ is skew-symmetric, $g(q) \in \Re^n$ is the vector of gravitational torques, $\tau \in \Re^n$ stands for the control input torques applied at the manipulator joints, $f_h \in \Re^m$ is the force applied to robot end-effector by human and $J(q) \in \Re^{m \times n}$ denotes the Jacobian matrix relating joint space and task space.

III. HUMAN–ROBOT INTERACTION INVOLVED CONTROL

In this section, we first identify three basic operation modes of the rehabilitative robotics based on the required capabilities. A controller consisting of a motion-related part (see Section III-A) and an interaction-related part (see Section III-B) is then introduced to realize the operation modes, while dealing with system uncertainties and changing human forces.

Based on the required capabilities of the rehabilitative robotics, i.e., customizability, adjustability, and safety, the three basic operation modes of the controller are identified as 1) a *human-dominant* mode in which the patient movements are trusted, encouraged thus only slightly interfered by the robot system, 2) a *robot-dominant* mode in which patient motion control is not reliable and desired movements are accomplished mostly by the assistance of the robot system, and 3) a *safety-stop mode* in which system end-effector is stopped due to the existence of conflicting human–robots movements and possible injuries to human if the robot stays active.

Human-dominant mode refers to the situation that human motion control has been partially restored. In this case, it is important that the affected human limb gains enough exercise through the therapeutic process, i.e., free limb motion should be allowed to a great extent. Meanwhile, certain level of speed regulation is beneficial to avoid abnormal movements that are too slow and too fast. Both of these two actions above can strengthen the accuracy and repeatability of human motion control in neuro-damaged patients' therapeutic process. Robot-dominant mode, on the other hand, stands for a scenario that human movements are either unreliable or inefficient. Thus, assistance from the robot system is always necessary to either finish the task or put the human limb back to the correct track, both by moving the system closer to a desired trajectory. Trajectory tracking with regulation on both position and speed of the system is suitable for this stage. Besides the two normal operation modes mentioned above, sometimes, the system may drift to an extent such that the position errors are too big and resulting control torques may incur damages to human body. In this case, the robotic system should be stopped. It is also reasonable that the faster the system moves, the faster it should be stopped in this dangerous situation. Thus, damping control should be employed here.

In practice, it is feasible and important for a normal rehabilitative robot to possess the capability to work in all of the three modes, determined by the system end-effector's instant position. As shown in Fig. 1, when the system end-effector is close to the desired trajectory, it is in human-dominant region (H-DR), when it is in the robot-dominant region (R-DR), the robot will help to push the whole system back to human-dominant region; however, when the end-effector is drifted into the outer safety-stop region (S-SR), the system is stopped.

To fit in the conditions of different patients and their various recovery status, the widths of human-dominant and R-DRs are expected to be adjustable. At the early stage of the therapeutic process, human movements are minor or totally unreliable. Thus, human-dominant region should be reduced to a very small area so that robot-assistance is constantly present. The rehabilitative robot actually works as an assistive robot in that case. On the other hand, when human motion control has been recovered, human region should be made larger to allow more freedom in human movements.

This scheme is also applicable to training of patients with spasticity. Similarly, depending on the severity of the spasticity,
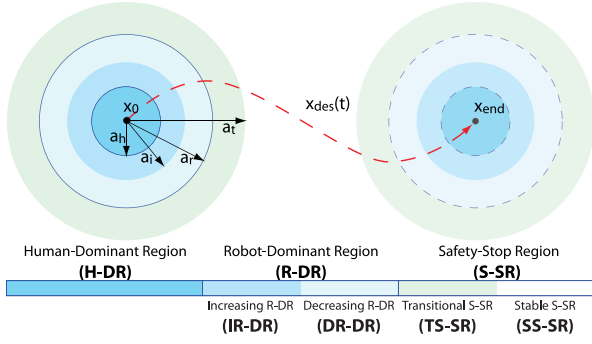
Fig. 1. Operation regions that move along the desired trajectory $x_{\text{des}}(t)$ determined by real-time position error $||\Delta x||$. From inside to outside, there are three main regions, namely human-dominant region (H-DR, $||\Delta x|| \in [0, a_h)$), robot-dominant region (R-DR, $||\Delta x|| \in (a_h, a_r]$), and safety-stop region (S-SR, $||\Delta x|| \in (a_r, +\infty)$). The increasing (IR-DR, $||\Delta x|| \in (a_h, a_i]$) and decreasing (DR-DR, $||\Delta x|| \in (a_i, a_r]$) subregions of R-DR are identified by increasing and decreasing stiffness (Section III-A.†2). The transitional subregion of S-SR (TS-SR, $||\Delta x|| \in (a_r, a_t]$) exists to ensure smooth transition from R-DR to stable S-SR (SS-SR, $||\Delta x|| \in (a_t, +\infty)$). See Section III-A.†1).

the sizes of various regions can be fine-tuned during initial trials. Patients with more severe spasticity should use larger R-DR so that reasonable amount of training can be received without constant stops in the safety-stop region. Actually, the desired region can be suspended if the patient enters safety-stop region to pause the training. The training can still be resumed by moving the arm back to the suspended region either through self-effort or with help.

To deal with the specific issues related to the rehabilitation robotics described by (1), the proposed controller is divided into two portions, a motion-related controller τ_m and an interaction-related controller τ_i, i.e.,

$$\tau = \tau_m + \tau_i \tag{2}$$

in which τ_m realizes the three main operation modes and deals with modeling uncertainties, and τ_i deals with conflicting human–robot movements. Together, the two also ensure the stability of the closed-loop system.

A. Motion-Related Controller

The motion-related controller includes a stiffness control (proportional control) term ((3) term $\mathfrak{a}$), a sliding control term ((3) term $\mathfrak{b}$) and an adaptive term ((3) term $\mathfrak{c}$). Stiffness control and sliding control terms together realize the three operation regions illustrated in Fig. 1, while the adaptive term deals with system uncertainties. The motion-related controller is expressed as

$$\tau_m = \underbrace{-\mathcal{M}^{\mathsf{T}}(x)J^{\mathsf{T}}(q)k_p(\delta x)\delta x}_{\text{term } \mathfrak{a}} \underbrace{-K_s s}_{\text{term } \mathfrak{b}}$$
$$+ \underbrace{Y_d(q, \dot{q}, \dot{q}_r, \ddot{q}_r)\hat{\theta}}_{\text{term } \mathfrak{c}} \tag{3}$$

where $q \in \Re^n$ and $J(q) \in \Re^n$ are the joint displacement vector and Jacobian matrix respectively as defined in (1); $x = [x_1, ..., x_m]^{\mathsf{T}} \in \Re^m$ ($m \leq 3$) is the position of the robot end-effector in task space, δx is a weighted position error, $\mathcal{M}(x) \in \Re^{n \times n}$ is a modifier matrix, $k_p(\delta x) \in \Re$ is a nonnegative

position-dependent stiffness, $K_s \in \Re^{n \times n}$ is a positive sliding control gain, $s \in \Re^n$ is a sliding vector, $q_r \in \Re^n$ is a virtual reference joint vector, $Y_d(q, \dot{q}, \dot{q}_r, \ddot{q}_r) \in \Re^{n \times h}$ is a regressor matrix, and $\hat{\theta} \in \Re^h$ is an estimate of the unknown dynamics parameter vector $\theta \in \Re^h$.

Different from classical proportional control, term $\mathfrak{a}$ uses a position-dependent gain $k_p(\delta x)$. Besides, instead of the *direct position error* $\Delta x = x - x_{\text{des}}$, in which $x_{\text{des}} = [x_{\text{des},1}, ..., x_{\text{des},m}]^{\mathsf{T}}$ denotes the desired end-effector trajectory in task space, *a weighted position error* δx is used, which is defined as

$$\delta x = x - x_d \tag{4}$$

where x_d is a *weighted trajectory* expressed as

$$x_d = x_i + w(\Delta x)(x_{\text{des}} - x_i) = x_i + w(\Delta x)x_v \tag{5}$$

in which x_i is a *time-invariant* reference position, x_v is the *time-varying* part of x_d, and $w(\Delta x)$ is a Δx-based weight vector. Note that when $w(\Delta x) = 1$, $x_d = x_{\text{des}}$; when $w(\Delta x) = 0$, $x_d = x_i$, and $\dot{x}_d = 0$.

The position-dependence of k_p and the addition of $w(\Delta x)$ to desired trajectory together realize the three main operation modes. The *modifier* matrix $\mathcal{M}(x)$ is added to eliminate the use of $\ddot{x}$ in the controller, which emerges due to the usage of $w(\Delta x)$ in x_d, for noise reduction in implementation. The modifier matrix is defined as

$$\mathcal{M}(x) = \mathbb{I}_n - J^+(q)A(x)J(q) \tag{6}$$

where $\mathbb{I}_n$ is a $n \times n$ identity matrix, $J^+(q)$ is the pseudoinverse of $J(q)$, $A(x) \in \Re^{m \times m}$ is a transition matrix defined as

$$A(x) = \begin{bmatrix} \dfrac{\partial w}{\partial x_1}x_{\text{des},1} & \cdots & \dfrac{\partial w}{\partial x_m}x_{\text{des},1} \\ \vdots & \ddots & \vdots \\ \dfrac{\partial w}{\partial x_1}x_{\text{des},m} & \cdots & \dfrac{\partial w}{\partial x_m}x_{\text{des},m} \end{bmatrix}. \tag{7}$$

The use of position-dependent stiffness k_p, weight factor $w(\Delta x)$, and modifier matrix $\mathcal{M}$ also applies to the sliding vector s in term $\mathfrak{b}$, which is proposed correspondingly as

$$s = \dot{q} - \dot{q}_r$$
$$= \dot{q} - \mathcal{M}^{-1}(x)[J^+(q)\dot{x}_f - \alpha J^+(q)k_p(\delta x)\delta x] \tag{8}$$

where α is a constant, q_r is a *virtual joint reference vector*, x_f is a *virtual position reference vector* defined as $\dot{x}_f = w(\Delta x)\dot{x}_{\text{des}} - A(x)\dot{x}_{\text{des}}$.

The regressor $Y_d(q, \dot{q}, \dot{q}_r, \ddot{q}_r)$ in term $\mathfrak{c}$ is defined by

$$M(q)\ddot{q}_r + \left[\frac{1}{2}\dot{M}(q) + S(q, \dot{q})\right]\dot{q}_r + g(q) = Y_d(q, \dot{q}, \dot{q}_r, \ddot{q}_r)\theta$$

according to the linear-in-parameters property [25] of the system dynamics. By using this property, the vector of unknown system parameters θ can be estimated by the update law

$$\dot{\hat{\theta}} = -LY_d^{\top}(q, \dot{q}, \dot{q}_r, \ddot{q}_r)s \tag{9}$$

where $L \in \Re^{h \times h}$ is a positive-definite and nonsingular square matrix gain.

Note that this controller works with $m \leq 3$. However, for better presentation of the controller characteristics, $m = 2$ is

used mostly in the graphic illustrations. The 3-D case will be later discussed and demonstrated by simulation.

At any instant time t when a neuro-damage-affected human limb is in the process of finishing an action with the help of the robotic system, based on the direct position error Δx between end-effector position $x(t)$ and desired position $x_{\text{des}}(t)$, the workspace is divided into three portions: human-dominant region with radius a_h, R-DR with outer radius a_r, and safety-stop region where human safety will be compromised if robotic assistance is active. These three regions move along the desired trajectory together with instant $x_{\text{des}}(t)$ as shown in Fig. 1.

To meet these requirements of operation, certain conditions need to be satisfied. For proportional control term $-\mathcal{M}^{\intercal}(x)J^{\intercal}(q)k_p(\delta x)\delta x$ in (3), $k_p(\delta x)$ is strictly asserted to zero in human-dominant region and nonzero in R-DR. Besides, with the increase of position error δx inside the robot region, it is reasonable for $k_p(\delta x)$ to ramp up to rapidly restore the system back to the previous region. However, the value of $-\mathcal{M}^{\intercal}(x)J^{\intercal}(q)k_p(\delta x)\delta x$ will grow to a point where the control input torque becomes damaging to human body. Similar problem happens to term $-K_s s$. These concerns for human safety nurture the necessity of the third region safety-stop region. In this region, $k_p(\delta x)$ is again set to zero to cease stiffness control, and damping will be introduced to stop the motion.

These design requirements are realized by the employment of the *position-dependent trajectory weight vector* (†1) and the *position-dependent stiffness* (†2).

†1 The *position-dependent weight vector* $w(\Delta x)$ is added to realize velocity tracking in human and R-DRs and damping in safety-stop region by asserting $\dot{x}_d(t) = 0$, i.e., weight vector $w(\Delta x)$ in (5) meets requirements

$$w(\Delta x) = \begin{cases} 1, & \text{H-DR} \cup \text{R-DR} \\ 0, & \text{S-SR} \end{cases}$$

in which the symbol $\cup$ denotes union operation.

To ensure smooth transition instead of asserting $w(\Delta x) = 0$ in whole safety-stop region, a *transitional safety-stop subregion* (TS-SR) is added at the outer edge of R-DR, in which $w(\Delta x)$ smoothly changes from 1 to 0. The subregion in which $w(\Delta x) = 0$ is then named as *stable safety-stop region* (SS-SR). This smooth definition of $w(\Delta x)$ is equation (10), as shown on the bottom of the page, where a_r is a positive constant standing for outer radius of R-DR; $a_t = a_r + h_t$ stands for outer radius of transitional safety-stop region, with a small constant of design h_t denoting the width of the region. With this definition, an illustration of the shape of $w(\Delta x)$ for $m = 2$ is available in Fig. 2.

While realizing velocity tracking and damping in different regions, the addition of $w(\Delta x)$ also potentially introduces $\ddot{x}$ into the controller if we define the sliding vector classically
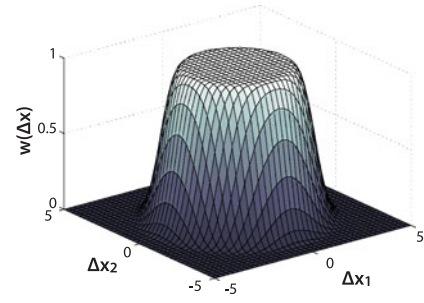

Fig. 2.   Illustration of the weight factor w versus Δx for $m = 2$, with $a_r = 2, a_t = 4.5$. $w = 1$ when $||\Delta x|| \in [0, a_r]$ in the human-dominant region (H-DR) and robot-dominant region (R-DR); $w = 0$ when $||\Delta x|| \in (a_t, +\infty)$ in the stable safety-stop region (SS-SR). w smoothly transits from 1 to 0 when $||\Delta x|| \in (a_r, a_t]$ in the transitional safety-stop region (TS-SR).

as

$$s_q = \dot{q} - J^+(q)\dot{x}_d + \alpha J^+(q)k_p(\delta x)\delta x \qquad (11)$$

due to double differentiation of $w(\Delta x)$ in $x_d(t)$. s_q here is labeled as an *intermediate sliding vector*. To avoid the use of acceleration in the controller, the modifier matrix $\mathcal{M}$ defined in (6) is used as detailed below.

Differentiating (5) with respect to time and using (7), we have

$$\begin{aligned} \dot{x}_d &= \dot{w}(\Delta x)x_{\text{des}} + w(\Delta x)\dot{x}_{\text{des}} \\ &= A(x)\dot{x} - A(x)\dot{x}_{\text{des}} + w(\Delta x)\dot{x}_{\text{des}} \\ &= A(x)\dot{x} + \dot{x}_f. \end{aligned} \qquad (12)$$

From (6) and (12), the intermediate vector s_q defined in (11) can be rewritten as

$$\begin{aligned} s_q &= [\mathbb{I}_n - J^+(q)A(x)J(q)]\dot{q} - J^+(q)\dot{x}_f \\ &\quad + \alpha J^+(q)k_p(\delta x)\delta x \\ &= \mathcal{M}\dot{q} - J^+(q)\dot{x}_f + \alpha J^+(q)k_p(\delta x)\delta x. \end{aligned} \qquad (13)$$

Now, it is clear that the sliding vector that is defined as

$$s = \mathcal{M}^{-1}(x)s_q \qquad (14)$$

can be rewritten into the format of (8), in which the reference joint variable time derivative $\dot{q}_r = \mathcal{M}^{-1}(x)\left[J^+(q)\dot{x}_f - \alpha J^+(q)k_p(\delta x)\delta x\right]$ includes no $\dot{x}$ and therefore the term $\ddot{x}$ is eliminated in $\ddot{q}_r$ and, hence, control input τ.

With this weighted desired trajectory above, considering the fact that $A(x) = 0_{m \times m}$ ($m \times m$ zero matrix) and, thus, $\mathcal{M}(x) = \mathbb{I}_n$ for $w = 0$ or 1 (i.e., in human-dominant, robot-dominant, and stable safety-stop regions), and the design

$$w(\Delta x) = \begin{cases} 1, & ||\Delta x|| \in [0, a_r], \text{ i.e., H-DR} \cup \text{R-DR} \\ 1 - \dfrac{\{[||\Delta x||^2/a_t^2 - 1]^4 - [a_r^2/a_t^2 - 1]^4\}^4}{[a_r^2/a_t^2 - 1]^{4^2}}, & ||\Delta x|| \in (a_r, a_t], \text{ i.e., TS-SR} \\ 0, & ||\Delta x|| \in (a_t, +\infty), \text{ i.e., SS-SR} \end{cases} \qquad (10)$$

requirement that $k_p(\delta x) = 0$ in human-dominant and safety-stop regions, the sliding control portion is

$$-K_s s = -K_s \mathcal{M}^{-1}(x)[\dot{q} - J^+(q)\dot{x}_d + \alpha J^+(q)k_p(\delta x)\delta x]$$

$$= \begin{cases} -K_s[\dot{q} - J^+(q)\dot{x}_{\text{des}}], & ||\Delta x|| \in [0, a_h] \\ & \text{i.e., H-DR} \\ -K_s[\dot{q} - J^+(q)\dot{x}_{\text{des}} & ||\Delta x|| \in (a_h, a_r] \\ +\alpha J^+(q)k_p(\delta x)\delta x], & \text{i.e., R-DR} \\ -K_s \mathcal{M}^{-1}(x)[\dot{q} - J^+(q)\dot{x}_d], & ||\Delta x|| \in (a_r, a_t] \\ & \text{i.e., TS-SR} \\ -K_s \dot{q}, & ||\Delta x|| \in (a_t, +\infty) \\ & \text{i.e., SS-SR} \end{cases}$$

(15)

which implements speed control in human-dominant region and transitional safety-stop region, trajectory tracking control in R-DR and damping control in stable safety-stop region.

†2 The *position-dependent stiffness* $k_p(\delta x)$ is used instead of a constant one so that proportional control is only used in R-DR, i.e.,

$$k_p(\delta x) = \begin{cases} 0, & \text{H-DR} \\ \text{positive value}, & \text{R-DR} \\ 0, & \text{S-SR.} \end{cases}$$

With the addition of $w(\Delta x)$ to facilitate the system passivity and stability, weighted error δx is used for proportional control portion instead of director error Δx.

In order to obtain a continuous and differentiable stiffness that meets the requirements above, an auxiliary function is first defined as

$$f_p(\delta x) = 1 - \exp[-a(||\delta x||^2 - a_h^2)] \qquad (16)$$

and the position-dependent stiffness is described accordingly as

$$k_p(\delta x) = k_1[\max(0, f_p(\delta x))]^2 \exp[-a(||\delta x||^2 - a_h^2)] \qquad (17)$$

in which a and k_1 are positive constants of design, and a_h is the radius of human-dominant region as mentioned earlier. An illustration of the shape of this stiffness function is available in Fig. 3. Note that there are two subregions for R-DR, an increasing one (IR-DR) and a decreasing one (DR-DR). The outer radius of the former a_i is adjustable by a and a_h according to

$$a_i = \left\{ ||\delta x|| : \frac{\partial k_p(\delta x)}{\partial \delta x} = 0, ||\delta x|| > a_h \right\}.$$

The outer radius of the decreasing region, as well as the whole R-DR a_r is also controllable by k_1, a, and a_h. Supposing the controller processor has a minimum distinguishable signal size or quantization step size p, i.e., a scalar signal $y \equiv 0$ if $|y| < p$, then a_r is determined by $a_r = \{ ||\delta x|| : k_p(\delta x) = p, ||\delta x|| > a_i \}$.

Note that human-dominant region provides the patients with opportunity to exercise and R-DR guarantees human action correctness and reinforces human motion control. Thus, the existence of both regions is a key feature to the rehabilitative
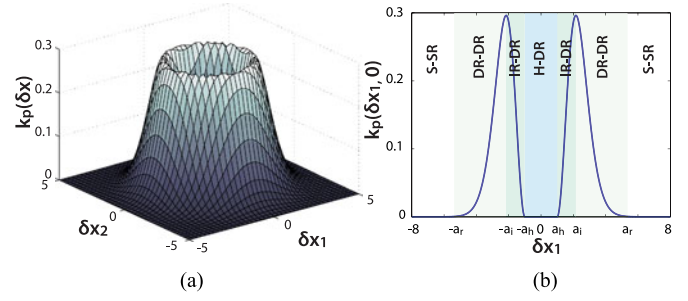

Fig. 3. Illustration of the position-dependent stiffness k_p versus δx for $m = 2$, with $a_h = 1$, $a = 0.3$, $k_1 = 2$. (a) A 3-D view. (b) A 2-D view: intersection of k_p and surface $\delta x_2 = 0$. When $||\delta x|| \in [0, a_h] \cup (a_r, +\infty)$ in human-dominant region (H-DR) and safety-stop region (S-SR), $k_p = 0$; When $||\delta x|| \in (a_h, a_r]$ in R-DR, $k_p > 0$. Increasing robot-dominant region (IR-DR) denotes the subregion of R-DR in which $\frac{\partial k_p}{\partial ||\delta x||} > 0$, i.e., k_p increases as $||\delta x||$ increases. Decreasing robot-dominant region (DR-DR) denotes the subregion with $\frac{\partial k_p}{\partial ||\delta x||} < 0$.

process and the relative sizes of them should reflect the recovery extent of human motion control. When human limb movement is less reliable, a_h should be set smaller to ensure less human free motion and more robotic assistance; similarly, when human gains better motion control, a_h should be set larger to allow more human exercise and little robot help as needed to further boost patients' recovery. When a_h is set to zero, the system is robot-dominant, which is useful at the beginning, i.e., *robot-assisting* stage, of the therapy. Besides, the general width of R-DR can be easily controlled by a. As a increases, the width of R-DR drops rapidly.

The fixed reference position x_i of the weighted trajectory x_d is chosen to be sufficiently far away from the desired path x_{des} so that $||\Delta x|| > a_r$ always guarantees $||\delta x|| > a_r$ in operation, i.e., in this region $k_p(\delta x) = 0$.

With the $k_p(\delta x)$ and x_i defined above, the stiffness control portion is

$$-\mathcal{M}^\mathsf{T}(x)J^\mathsf{T}(q)k_p(\delta x)\delta x =$$

$$\begin{cases} 0, & ||\Delta x|| \in [0, a_h] \\ & \text{i.e., H-DR} \\ -J^\mathsf{T}(q)k_p(\delta x)\delta x, & ||\Delta x|| \in (a_h, a_r] \\ & \text{i.e., R-DR} \\ 0, & ||\Delta x|| \in (a_r, +\infty) \\ & \text{i.e., S-SR} \end{cases}$$

(18)

in which proportional control with nonzero stiffness is deployed in R-DR only.

With stiffness and desired trajectory defined above, τ_m is proposed as (3). Note that $J^+(q)$ and $\mathcal{M}(x) = \mathbb{I}_n - J^+(q)A(x)J(q)$ are involved in the controller which potentially causes issues at the singularities of them. For $J^+(q)$, it is handled by specifying a desired trajectory $x_{\text{des}}(t)$ such that all singularities are in stable safety-stop region, in which case $kp(\delta x)$ and $\dot{x}_d$ already reduce to zero and $\mathcal{M} = \mathbb{I}_n$, the motion related controller reduces to

$$\tau_m = -K_s \dot{q} + Y_d(q, \dot{q}, 0, 0)\hat{\theta}$$

thus the singularity issue of the controller due to $J(q)$ is contained. Since matrix A is $0_{m \times m}$ in human-dominant,

robot-dominant, and stable safety-stop regions, $\mathcal{M} = \mathbb{I}_n$ is always invertible in these main operating regions. For the case that $A \neq 0_{m \times m}$ in the transitional safety-stop region, since $\mathcal{M} = \mathbb{I}_n - J^+(q)A(x)J(q)$ is a general matrix that varies according to robot kinematics and tasks, it is difficult to derive a general analytic inverse matrix. The inverse matrix has to be analyzed according to the particular robot structure and tasks to contain singularity issue (if any) by trajectory planning or saturating the inverse matrix. Since transitional safety-stop region is a very narrow zone between robot-dominant and stable safety-stop regions that only for the purpose of smoothing the transition, saturating $\mathcal{M}^{-1}$ will not affect the performance in the three main regions.

B. Interaction-Related Controller

The interaction-related controller has two objectives, to ensure the closed-loop system stability together with the motion-related controller, and to reduce the conflicts between human and robot movements. τ_i is proposed as a function of the human interaction force f_h, the position error Δx, and the sliding vector s as

$$\tau_i = J^\mathsf{T}(q)C_x(f_h, \Delta x, s) \tag{19}$$

in which C_x is the task-space interaction controller.

Research work on human science [26] has shown that human central nervous system may use a composite variable [25] consisting of tracking errors and their temporal derivatives in motion control. This composite variable can serve as either an error prediction or a criterion to be minimized. In a limb rehabilitative process assisted by a robot system, when human limb is well functioning and the robot is unactuated, the interaction force received by the robot should be fully responsible for achieving both position and speed objectives set for it, i.e., minimizing the composite variable. For the controller proposed in this paper, this composite variable is represented by the task space sliding vector s_x, a combination of the transformed position and velocity errors as

$$
s_x = J(q)s = J(q)\mathcal{M}^{-1}(x)s_q
$$
$$
= \begin{cases}
\delta \dot{x}, & \|\Delta x\| \in [0, a_h], \quad \text{i.e., H-DR} \\
\delta \dot{x} + \alpha k_p(\delta x)\delta x, & \|\Delta x\| \in (a_h, a_r], \quad \text{i.e., R-DR} \\
J(q)\mathcal{M}^{-1}(x)s_q, & \|\Delta x\| \in (a_r, a_t], \quad \text{i.e., TS-SR} \\
\dot{x}, & \|\Delta x\| \in (a_t, +\infty), \quad \text{i.e., SS-SR.}
\end{cases}
\tag{20}
$$

In this case, the direction of resulting force $C_x(f_h, \Delta x, s) + f_h$ should be aligned with the opposite of this variable.

In the safety-stop region, since the whole system is supposed to be damped to static status, f_h is directly canceled by the controller. On the other hand, in human-dominant region, human movements are considered reliable to certain extent, and the controller is then introduced with three modes based on $\gamma \in [0, \pi]$, which is the magnitude of directional difference between vector $-s_x$ and f_h as demonstrated in Fig. 4, to encourage active human movements. When f_h orientates close enough to $-s_x$ with $\gamma \leq \beta$, in which β is a threshold adjustable in $[0, \frac{\pi}{2}]$, human motion is considered reliable, and the interaction force is retained. This region is called the *retaining region (RR)*. Otherwise, if f_h direction is out of this area, but still maintains an angle difference less than σ (adjustable in $[0, \frac{\pi}{2}]$) with one retaining region edge (denoted by unit vector either $-s'_{x1}$ or
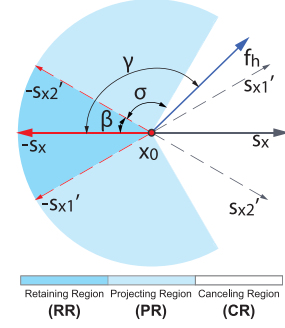

Fig. 4. Interaction force handling regions determined by the magnitude of directional difference γ between interaction force f_h and the opposite of task space sliding vector s_x. When $\gamma \leq \beta$, $\beta \in [0, \frac{\pi}{2}]$, system is in retaining region (RR); when $\gamma \in (\beta, \beta + \sigma]$, $\sigma \in [0, \frac{\pi}{2}]$, system is in projecting region (PR); otherwise, system is in canceling region (CR).

$-s'_{x2}$), it is in the *projecting region (PR)* and is projected to whichever edge that is closer. Other than these two regions, f_h is considered wrongly orientated, i.e., human movements are not reliable. Interaction is directly canceled and this area is the *canceling region (CR)*. Finally, R-DR serves as a transition area.

With these discussions, the interaction-related controller is developed such that

$$
C_x(f_h, \Delta x, s) + f_h
$$
$$
= \begin{cases}
\mu_s(s)c_x(f_h), & \|\Delta x\| \in [0, a_h], \quad \text{i.e., H-DR} \\
\mu_s(s)\mu_x(\Delta x)c_x(f_h), & \|\Delta x\| \in (a_h, a_r], \quad \text{i.e., R-DR} \\
0, & \|\Delta x\| \in (a_r, +\infty), \quad \text{i.e., S-SR}
\end{cases}
\tag{21}
$$

where

$$
c_x(f_h)
$$
$$
= \begin{cases}
f_h, & \gamma \in [0, \beta], \quad \text{i.e., RR} \\
-s'_x \|f_h\| \cos^2\left[\dfrac{(\gamma - \beta) \cdot \pi}{2\sigma}\right], & \gamma \in (\beta, \beta + \sigma], \quad \text{i.e., PR} \\
0, & \gamma \in (\beta + \sigma, \pi], \quad \text{i.e., CR}
\end{cases}
\tag{22}
$$

with $-s'_x$ equals to $-s'_{x1}$ or $-s'_{x2}$, whichever has a closer direction with f_h. The term

$$
\mu_x(\Delta x) = \sin^2\left[\frac{(a_r - \|\Delta x\|) \cdot \pi}{2(a_r - a_h)}\right], \|\Delta x\| \in (a_h, a_r] \text{ only}
\tag{23}
$$

is a position-based coefficient to ensure smooth transition between human-dominant and safety-stop regions; the saturation function

$$
\mu_s(s) = \begin{cases}
1, & \|s_x\| \geq w_s \\
\sin^2\left(\dfrac{\|s_x\|\pi}{2w_s}\right), & \|s_x\| < w_s
\end{cases}
$$

is added as a second coefficient of $c_x(f_h)$ to assert force-dominant controller when s has a norm bigger than a small positive constant w_s, and sliding-vector-dominant controller otherwise so that the controller is smoothed at $s = 0$. Without

$\mu_s(s)$, the resulting force magnitude $||C_x + f_h||$ is discontinuous at $s_x = 0$, while it is smooth and continuous with $\mu_s(s)$. Instead of direct projection to $-s'_x$ direction, a second order projection $\cos^2(\bullet)$ is used in the controller to ensure its differentiability.

With definitions above, the control result $C_x(f_h, \Delta x, s) + f_h$ is uniformly continuous on s, Δx and also f_h, and the term

$$s^\mathsf{T} J^\mathsf{T}(q)[C_x(f_h, \Delta x, s) + f_h] = s_x^\mathsf{T}[C_x(f_h, \Delta x, s) + f_h]$$

$$= \begin{cases} \mu_s(s)s_x^\mathsf{T} c_x(f_h), & ||\Delta x|| \in [0, a_h], & \text{i.e., H-DR} \\ \mu_s(s)\mu_x(\Delta x)s_x^\mathsf{T} c_x(f_h), & ||\Delta x|| \in (a_h, a_r], & \text{i.e., R-DR} \\ 0, & ||\Delta x|| \in (a_r, +\infty), & \text{i.e., S-SR} \end{cases} \tag{24}$$

where

$$s_x^\mathsf{T} c_x(f_h)$$

$$= \begin{cases} -||s_x||||f_s|| \cos(\gamma), & \gamma \in [0, \beta] \\ & \text{i.e., RR} \\ -||s_x||||f_s|| \cos(\beta) \cos^2 \left[\frac{(\gamma-\beta)\cdot\pi}{2\sigma} \right], & \gamma \in (\beta, \beta+\sigma] \\ & \text{i.e., PR} \\ & \gamma \in (\beta+\sigma, \pi] \\ 0, & \text{i.e., CR.} \end{cases} \tag{25}$$

Since $\beta \le \frac{\pi}{2}$, (24) is never greater than zero.

When $m = 3$, all mathematical descriptions of the controller still hold, while the shapes of various regions change from 2-D to 3-D. For motion-related controller, human-dominant region changes from a disk to a ball and R-DR changes from a ring to a hollow ball. For interaction-related part, regions change from circular sectors into cones.

IV. Passivity and Stability of the System

In this section, passivity of the closed-loop system with the proposed controller and convergence of various state variables in different operation modes are analyzed using Lyapunov method. It is shown that system passivity can be ensured and the position of the end-effector either converges to the human-dominant region, or stops in safety-stop region depending on the interactions between the human and robot.

A. System Passivity

By using (8) and substituting (2), (3), and (19) into (1), the closed-loop system dynamic equation becomes

$$M(q)\dot{s} + \left[\frac{1}{2}\dot{M}(q) + S(q, \dot{q}) \right] s + \mathcal{M}^\mathsf{T}(x)J^\mathsf{T}(q)k_p(\delta x)\delta x$$

$$+ K_s s + Y_d(q, \dot{q}, \dot{q}_r, \ddot{q}_r)\Delta\theta$$
$$= J^\mathsf{T}(q)[C_x(f_h, \Delta x, s) + f_h] \tag{26}$$

where $\Delta\theta = \theta - \hat{\theta}$. With no interaction-related controller asserted, i.e., $C_x(f_h, \Delta x, s) = 0$, the time integral of the inner product between an output $y = s$ and (26) yields

$$\int_0^t s^\mathsf{T}(\varsigma)J^\mathsf{T}(\varsigma)f_h(\varsigma)d\varsigma$$

$$= \int_0^t \left\{ s^\mathsf{T}(\varsigma)M(q(\varsigma))\dot{s}(\varsigma) + s^\mathsf{T}(\varsigma)\left[\frac{1}{2}\dot{M}(\varsigma) + S(\varsigma) \right] s(\varsigma) \right.$$

$$+ [\dot{q}(\varsigma) - J^+(\varsigma)\dot{x}_d(\varsigma))]^\mathsf{T}[\mathcal{M}^{-1}(\varsigma)]^\mathsf{T}\mathcal{M}^\mathsf{T}(\varsigma)J^\mathsf{T}(\varsigma)k_p(\varsigma)\delta x(\varsigma)$$

$$+ [\mathcal{M}^{-1}(\varsigma)\alpha J^+(\varsigma)k_p(\varsigma)\delta x(\varsigma)]^\mathsf{T}\mathcal{M}^\mathsf{T}(\varsigma)J^\mathsf{T}(\varsigma)k_p(\varsigma)\delta x(\varsigma)$$

$$\left. + s^\mathsf{T}(\varsigma)K_s s(\varsigma) + s^\mathsf{T}(\varsigma)Y_d(\varsigma)\Delta\theta(\varsigma) \right\}d\varsigma. \tag{27}$$

By using the skew-symmetric property of $S(q, \dot{q})$, the first two terms on the right-hand side of (27) can be expressed as

$$\int_0^t \left\{ s^\mathsf{T}(\varsigma)M(q(\varsigma))\dot{s}(\varsigma) + s^\mathsf{T}(\varsigma)\left[\frac{1}{2}\dot{M}(\varsigma) + S(\varsigma) \right] s(\varsigma) \right\}d\varsigma$$

$$= \frac{1}{2}s^\mathsf{T}(t)M(q(t))s(t) - \frac{1}{2}s^\mathsf{T}(0)M(q(0))s(0). \tag{28}$$

The third term of (27) can be simplified as

$$\int_0^t \left\{ [\dot{q}(\varsigma) - J^+(\varsigma)\dot{x}_d(\varsigma))]^\mathsf{T}[\mathcal{M}^{-1}(\varsigma)]^\mathsf{T} \right.$$

$$\left. \mathcal{M}^\mathsf{T}(\varsigma)J^\mathsf{T}(\varsigma)k_p(\varsigma)\delta x(\varsigma) \right\}d\varsigma$$

$$= \int_0^t \left\{ [J(\varsigma)(\dot{q}(\varsigma) - J^+(\varsigma)\dot{x}_d(\varsigma))]^\mathsf{T}k_p(\varsigma)\delta x(\varsigma) \right\}d\varsigma$$

$$= \int_0^t \left\{ [\dot{x}(\varsigma) - \dot{x}_d(\varsigma)]^\mathsf{T}k_p(\varsigma)\delta x(\varsigma) \right\}d\varsigma$$

$$= \int_0^t \left\{ \delta\dot{x}^\mathsf{T}(\varsigma)k_p(\varsigma)\delta x(\varsigma) \right\}d\varsigma$$

$$= \int_0^{\delta x} \left\{ d(\delta x^\mathsf{T})k_p(\delta x)\delta x \right\}\big|_0^t$$

$$= P_t(\delta x(t)) - P_t(\delta x(0)) \tag{29}$$

where the pseudopotential function $P_t(\delta x)$ is expressed as

$$P_t(\delta x) = \frac{1}{6a}k_1[\max(0, f_p(\delta x))]^3.$$

The last step of (29) comes from the fact that

$$\frac{\partial P_t(\delta x)}{\partial \delta x} = \frac{1}{6a} \cdot k_1 \cdot 3$$

$$\cdot [\max(0, f_p(\delta x))]^2 \exp[-a(||\delta x||^2 - a_h^2)]a \cdot 2 \cdot \delta x$$

$$= k_p(\delta x)\delta x$$

and, thus,

$$\int_0^{\delta x} \left\{ d(\delta x^\mathsf{T})k_p(\delta x)\delta x \right\} = P_t(\delta x).$$

Next, the fourth term can be written as

$$\int_0^t \left\{ [\mathcal{M}^{-1}(\varsigma)\alpha J^+(\varsigma)k_p(\varsigma)\delta x(\varsigma)]^\mathsf{T} \right.$$

$$\left. \mathcal{M}^\mathsf{T}(\varsigma)J^\mathsf{T}(\varsigma)k_p(\varsigma)\delta x(\varsigma) \right\}d\varsigma$$

$$= \int_0^t \alpha[\delta x(\varsigma)]^\mathsf{T}k_p(\varsigma)^2\delta x(\varsigma)d\varsigma. \tag{30}$$
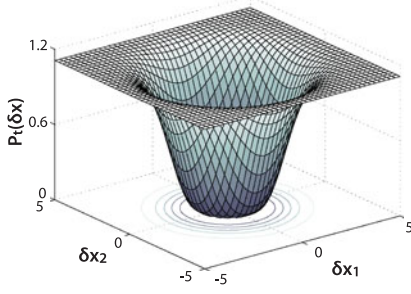
Fig. 5. Illustration of the pseudoenergy versus the weighted position error δx for $m = 2$: $a_h = 1, a = 0.3, k_1 = 2$. For $||\delta x|| \in [0, a_h]$, i.e., human-dominant region, $P_t(\delta x) = 0$. For $||\delta x|| \in (a_r, +\infty)$, i.e., safety-stop region, $P_t(\delta x)$ is saturated. For $||\delta x|| \in (a_h, a_r]$ in the R-DR, $P_t(\delta x)$ smoothly changes from 0 to its maximum.

Then, based on the system parameter estimate update law (9), the final term of (27) can be expressed as

$$\int_0^t \{s^{\mathsf{T}}(\varsigma)Y_d(\varsigma)\Delta\theta(\varsigma)\}d\varsigma$$

$$= \int_0^t \{\Delta\dot{\theta}(\varsigma)L^{-1}\Delta\theta(\varsigma)\}d\varsigma$$

$$= \frac{1}{2}\Delta\theta(t)^{\mathsf{T}}L^{-1}\Delta\theta(t) - \frac{1}{2}\Delta\theta(0)^{\mathsf{T}}L^{-1}\Delta\theta(0). \quad (31)$$

Combining (28)–(31), we have

$$\int_0^t s^{\mathsf{T}}(\varsigma)J^{\mathsf{T}}(\varsigma)f_h(\varsigma)d\varsigma$$

$$= \underbrace{V(t) - V(0)}_{\text{Stored Energy}} + \underbrace{\int_0^t W(\varsigma)d\varsigma}_{\text{Dissipated Energy}} \quad (32)$$

where

$$V = \frac{1}{2}s^{\mathsf{T}}M(q)s + P_t(\delta x) + \frac{1}{2}\Delta\theta L^{-1}\Delta\theta \quad (33)$$

and

$$W = s^{\mathsf{T}}K_s s + \alpha\delta x^{\mathsf{T}}k_p^2(\delta x)\delta x. \quad (34)$$

The pseudopotential $P_t(\delta x)$, as illustrated in Fig. 5, has no local minimum and only global minimum inside human-dominant region, and has

$$P_t(\delta x) \geq 0.$$

Then, since instant stored energy $V(t)$ in the system is composed of quadratic forms $\frac{1}{2}\Delta\theta L^{-1}\Delta\theta$, $s^{\mathsf{T}}M(q)s$ and the nonnegative $P_t(\delta x)$, it is thus clear that

$$V(t) \geq 0. \quad (35)$$

Next, the energy dissipation rate $W(s, \dot{q})$ is nonnegative from (34). Therefore, we can prove the theorem as follows.

Theorem 1: The input $J^{\mathsf{T}}(q)f_h$ and output $y = s$ of the closed loop system described by (26) and (9) satisfy the passivity property.

Proof: Equation (32) can be written as

$$\int_0^t s^{\mathsf{T}}(\varsigma)J^{\mathsf{T}}(\varsigma)f_h(\varsigma)d\varsigma$$

$$= \underbrace{V(t) - V(0)}_{\text{Stored Energy}} + \underbrace{\int_0^t W(\varsigma)d\varsigma}_{\text{Dissipated Energy}}$$

$$\geq -V(0) = -k_0^2$$

in which k_0^2 is a nonnegative value denoting the initial system energy. Therefore, the input $J^{\mathsf{T}}(q)f_h$ and output $y = s$ have passive relationship. ∎

In practical rehabilitative robotic systems, due to the existence of human–robot interaction, the term $s^{\mathsf{T}}J^{\mathsf{T}}(q)f_h$ will not be zero, which may result in increase of errors and storage energy. This problem is solved by the interaction-related controller τ_i that leads to $s^{\mathsf{T}}J^{\mathsf{T}}(q)[C_x(f_h, \Delta x, s) + f_h] \leq 0$ as in (24). Therefore, it is established that

$$\dot{V} = -W' = -W + s^{\mathsf{T}}J^{\mathsf{T}}(q)[C_x(f_h, \Delta x, s) + f_h] \leq 0 \quad (36)$$

in which W' is the net energy dissipation rate.

B. Convergence

Different from the traditional control problem in which there are no external forces involved, the human–robot interaction may push the system end-effector into various regions. Therefore, the convergence of the state variables needs to be investigated depending on the robot end-effector position that the system starts in or enters. With the passivity conclusion, we can prove the following theory.

Theorem 2: The closed-loop system described by (26) and (9) guarantees the convergence of the position of end effector to the human-dominant region if it is in human or R-DRs. If position of the end-effector enters the stable safety-stop region, then it stops in this region.

Proof: For all cases, the function V represents a Lyapunov-like function, with $V \geq 0$ and $\dot{V} = -W' \leq 0$ from (35) and (36). Hence, it is clear that $V(t) \leq V(0)$, i.e., it is upper bounded. Since V is positive-definite in s and $\Delta\theta$, and $\dot{V}$ is negative semidefinite, we have that s and $\Delta\theta$ are bounded.

1) *Human-Dominant and Robot-Dominant Regions*

When robot end-effector enters or starts in these regions, it is known that

$$w(\Delta x) = 1, A(x) = 0_{m \times m}, \mathcal{M}^{-1}(x) = \mathbb{I}_n$$

$$V = \frac{1}{2}s^{\mathsf{T}}M(q)s + P_t(\delta x) + \Delta\theta^{\mathsf{T}}L^{-1}\Delta\theta$$

$$\dot{V} = -s^{\mathsf{T}}K_s s - \alpha\delta x^{\mathsf{T}}k_p^2(\delta x)\delta x$$

$$+ s^{\mathsf{T}}J^{\mathsf{T}}(q)[C_x(f_h, \Delta x, s) + f_h]$$

$$s = [\dot{q} - J^+(q)\dot{x}_{\text{des}} + \alpha J^+(q)k_p(\delta x)\delta x]$$

and the closed-loop dynamics is

$$M(q)\dot{s} + \left[\frac{1}{2}\dot{M}(q) + S(q, \dot{q})\right]s + K_s s + J^{\mathsf{T}}(q)k_p(\delta x)\delta x$$

$$+ Y_d(q, \dot{q}, \dot{q}_r, \ddot{q}_r)\Delta\theta - J^{\mathsf{T}}(q)[C_x(f_h, \Delta x, s) + f_h] = 0. \quad (37)$$

First, the boundedness of s and $\Delta\theta$ is already established. Next, $k_p(\delta x)\delta x$ is bounded by definition. $\dot{q}_r = J^+(q)[\dot{x}_f - \alpha k_p(\delta x)\delta x]$ is bounded if $\dot{x}_f = w(\Delta x)\dot{x}_{\text{des}} - A(x)\dot{x}_{\text{des}}$ is bounded, which is true if $\ddot{x}_{\text{des}}$ is bounded. Then, according to (8), $\dot{q}$ is also bounded. Since $\dot{q}$ is bounded and $J(q)$ is composed of trigonometric functions of q, $\dot{x} = J(q)\dot{q}$ is bounded. By using $\mathcal{M}(x)$, $\ddot{q}_r$ has been released from the dependence on $\ddot{x}$. Therefore, the boundedness of $\dot{x}$, $w(\Delta x)$, $\dot{w}(\Delta x)$, $\ddot{x}_{\text{des}}$, $\mathcal{M}(x)$, and $k_p(\delta x)\delta x$ suggests the boundedness of $\ddot{q}_r$. Thus, regressor $Y_d(q, \dot{q}, \dot{q}_r, \ddot{q}_r)$ is bounded. Next

$$\dot{V} = -2s^\mathsf{T} K_s \dot{s} - 2\alpha k_p^2(\delta x)\delta x^\mathsf{T}\delta\dot{x}$$
$$- 2\alpha\delta x^\mathsf{T} k_p(\delta x)\delta x \frac{\partial k_p(\delta x)}{\partial\delta x}\delta\dot{x} + \dot{s}^\mathsf{T} J^\mathsf{T}(q)$$
$$[C_x(f_h, \Delta x, s) + f_h]$$
$$+ s^\mathsf{T}\dot{J}^\mathsf{T}(q)[C_x(f_h, \Delta x, s) + f_h] + s^\mathsf{T} J^\mathsf{T}(q)$$
$$[\dot{C}_x(f_h, \Delta x, s) + \dot{f}_h]$$

is bounded due to the boundedness of $\dot{s}$, δx, $\delta\dot{x}$, $k_p(\delta x)$, $\frac{\partial k_p(\delta x)}{\partial\delta x}$, $\dot{C}_x(f_h, \Delta x, s)$ which is ensured by the definition of $C_x(f_h, \Delta x, s)$, and $\dot{f}_h$ due to the human motion capability limitation. According to Barbalat Lemma [25], $\dot{V} \to 0$ as $t \to \infty$, which implies $s \to 0$ and $k_p(\delta x)\delta x \to 0$ as $t \to \infty$. Thus, it is clear that $\dot{q} - J^+(q)\dot{x}_{\text{des}} \to 0$ as $t \to \infty$. We then have, $\dot{x} \to \dot{x}_{\text{des}}$, and $x \to$ H-DR. Therefore, velocities of the robot inside human-dominant or R-DRs converge to the desired ones $\dot{x}_{\text{des}}(t)$ and its end-effector goes to human-dominant region with radius a_h unless some strong external interference force it into the safety-stop region, in which case the analysis will be detailed in the next section.

2) *Safety-Stop Region*

If the robot end-effector enters this region accidentally or starts within it, it is known that $C_x(f_h, \Delta x, s) + f_h = 0$, $k_p(\delta x)\delta x = 0$, and $P_t(\delta x) = P_{t,sat}$ with $P_{t,sat}$ representing the $P_t(\delta x)$ value in its saturation region, which yields

$$s = \begin{cases} \mathcal{M}^{-1}(x)[\dot{q} - J^+(q)\dot{x}_d], & \|\Delta x\| \in (a_r, a_t], \text{i.e., TS-SR} \\ \dot{q}, & \|\Delta x\| \in (a_t, +\infty), \text{i.e., SS-SR} \end{cases}$$

and

$$\dot{V} = \begin{cases} -[\dot{q} - J^+(q)\dot{x}_d]^\mathsf{T} K_s[\dot{q} - J^+(q)\dot{x}_d], & \|\Delta x\| \in (a_r, a_t] \\ -\dot{q}^\mathsf{T} K_s \dot{q}, & \|\Delta x\| \in (a_t, +\infty). \end{cases}$$
$$(38)$$

Similar to the analysis of human and R-DRs, with the assumption of bounded human input, it can be proved that $\dot{V} \to 0$ as $t \to \infty$ based on the definition of the controller. Therefore, in stable safety-stop region, $\dot{q} \to 0$ as $t \to \infty$, i.e., $\dot{x} \to 0$ as $t \to \infty$, due to the quadratic property of $\dot{V}$ on $\dot{q}$. It means that damping is realized in stable safety-stop region. On the other hand, in transitional subregion, as $t \to \infty$, $[\dot{q} - J^+(q)\dot{x}_d] \to 0$, i.e., $\dot{x} \to \dot{x}_d$. This means

velocity tracking toward $\dot{x}_d$ in the transitional region is realized.

Therefore, when the system is inside the stable stop region, the velocities converge to zero rapidly and the system stops inside this region unless it hits the transitional region first. If by any means, system enters the narrow transitional region, the system end-effector velocity converges to the weighted desired velocity, which leads the system into either robot-dominant or stable safety-stop regions. Since $w(\Delta x)$ reduces to zero, the weighted desired velocity also reduces to zero when system approaches the stable stop region. ∎

V. SIMULATION AND EXPERIMENTS

Simulation and experiments were performed to demonstrate the functionality and performance of the proposed controller. Simulation was based on a 3-DOF RRR-robot to demonstrate the controller capability in 3-D space, i.e., $m = 3$, and on curved trajectory (see Section V-A). Experiments were conducted on a system consisting of 2-DOF planar robot connected in series with a supported human arm to demonstrate the system capability in 2-D space (see Section V-B), i.e., $m = 2$. Results and discussions are also given.

A. Simulation

A 3-link RRR manipulator with end-effector subjected to external force to emulate human–robot interaction was used for simulation. The three links have lengths $l_1 = l_2 = l_3 = 0.5$ m, distances between their joints and respective center of masses $l_{c1} = l_{c2} = l_{c3} = 0.25$ m, moments of inertia $I_1 = I_2 = I_3 = \mathbb{I}_3$ kg $\cdot$ m^2, and masses $m_1 = m_2 = m_3 = 2$ kg. θ_1, θ_2 and θ_3 denote the angular positions of the three joints.

A circular desired trajectory, centered at $[x_{1c} x_{2c} x_{3c}]^\mathsf{T} = [0.5 0.5 0.5]^\mathsf{T}$ m, with orientation vectors $[x_{1a} x_{2a} x_{3a}]^\mathsf{T} = [\frac{1}{\sqrt{3}} \frac{1}{\sqrt{3}} \frac{1}{\sqrt{3}}]^\mathsf{T}$, $[x_{1b} x_{2b} x_{3b}]^\mathsf{T} = [\frac{1}{\sqrt{6}} - \frac{2}{\sqrt{6}} \frac{1}{\sqrt{6}}]^\mathsf{T}$, and radius $r = 0.3$ m, as described below was used for simulation:

$$x_{\text{des},i}(t) = x_{ic} + r\cos[2\pi\xi(t)]x_{ia}$$
$$+ r\sin[2\pi\xi(t)]x_{ib}, \ (i = 1, 2, 3)$$

in which the speed distribution function $\xi(t)$ was specified as

$$\xi(t) = \begin{cases} \frac{2t^2}{T^2}, & t \in [0, \frac{T}{2}] \\ 1 - \frac{2(T-t)^2}{T^2}, & t \in (\frac{T}{2}, T] \end{cases}$$

to ensure zero start and end velocities. $T = 15$ s is the total simulation duration. The time-invariant trajectory reference point was chosen as $x_i = [0\ 0\ 0]^\mathsf{T}$.

The control parameters used were $a_h = 0.05$ m, $h_t = 0.01$, $k_1 = 5\text{e}4$, $a = 200$, $\alpha = 0.5$, $K_s = 50 \cdot \mathbb{I}_3$, $L = 0_{4\times4}$, $\beta = 0$ rad, $\sigma = 0.5\pi$ rad, and $w_s = 0.01$. A constant force $f_h = [10\ 10\ 10]^\mathsf{T}$ N was applied to demonstrate the controller capability under human interference. The outer radius of R-DR was calculated as $a_r \approx 0.322$ m at $p = 0.1$ with the parameters provided. The initial joint position q_0 was set as $[2.3\ 2.7\ 1.2]^\mathsf{T}$ rad, which meant an initial end-effector position $x_0 = [0.5430\ 0.3698\ 0.6078]^\mathsf{T}$ m by forward kinematics. These initial position and desired trajectory were chosen such that the initial position error, $\Delta x_0 = 0.3366$ m, was larger than a_r, i.e., the system started in safety-stop region, as the path later approached x_0 and the system entered robot-dominant mode.
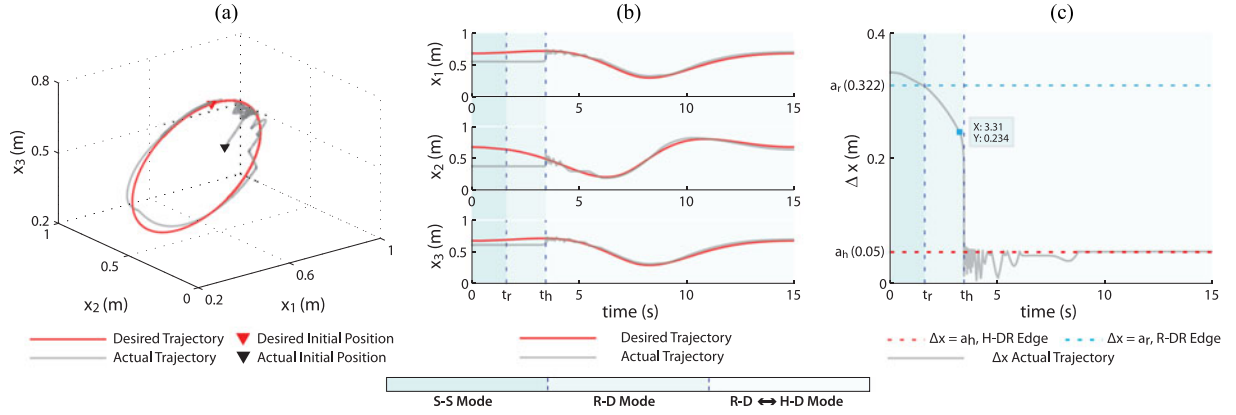
Fig. 6. Three-dimensional RRR-robot simulation results. (a) The desired and simulated trajectories in space. (b) The desired and simulated position trajectories of all three axis in time domain. (c) The instant distance of robot end-effector and desired central trajectory Δx in time. From (a) and (b), it is seen that the system end-effector started at a location far away from the initial desired position $x_{\mathrm{des}}(0)$ by design, which resulted in controller running safety-stop (S-S) mode at the beginning. As the desired trajectory x_{des} approached the end-effector later (intentionally by trajectory planning), controller entered robot-dominant (R-D) mode at t_r. At t_h, the system first entered human-dominant region and started H-D Mode. R-D mode occasionally was still activated in this period to ensure that the system stayed in human-dominant region.

Results of simulation, which include the desired and actual trajectories, velocities and position errors in time, are shown in Fig. 6.

At the beginning, being in safety-stop region, the device end-effector did not move (see Fig. 6.b), i.e., safety-stop control mode functioned correctly. Later, the device entered R-DR. Robot-dominant mode was then activated and the end-effector started to follow the desired human-dominant region. The region error with respect to the human-dominant region defined as $e_r(t) = \max(\|\Delta x(t)\| - a_h, 0)$ is available in Fig. 6(c).

From the simulation, the controller is able to work with 3-D highly curved desired trajectory in different operation modes with force interference. Note that due to the smooth transition between different operation regions of the controller, the behavior of the closed-loop system is not hard-switched at boundaries of various regions. Therefore, the end-effector did not start to move toward the human-dominant region immediately after it enters the R-DR (see Fig. 6(c)). Instead, it started to move when Δx is smaller ($t = 3.31$ s). After the system entered human-dominant region for the first time, e_r was not always exactly zero, but sometimes slightly bigger due to force interference, in which cases the system entered robot-dominant mode and was again pulled back to human region. From $t = 6.025$ s, when the system stabilized in human-dominant mode, the root mean square of region error e_r was about 8.86e–4 m.

B. Experiments

The proposed controller was implemented on an upper-limb rehabilitative robot that consisted of a 2-DOF planar robot manipulator connected to an unactuated planar arm support in series (see Fig. 7). A six-axis force sensor was installed between the robot end-effector and support to measure interaction forces.

The purpose of the experiments was to test the functionality of the controller and it was not a clinical or medical trial to test the biological response of patients. Thus, only one healthy subject (21 years, 1.72 m, 68 kg, male) was involved. Experimental methods employed were approved by the university and corresponding informed consent was provided by the subject.

In all experiments with data reported, the following parameters were used: $k_1 = 0.5$, $a = 0.3$, $K_s = 0.5 \cdot \mathbb{I}_2$, $\alpha = 1$,
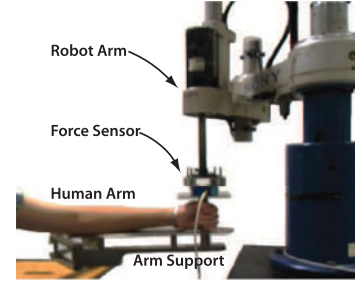

Fig. 7. Experimental testbed: An upper-limb rehabilitative robotics composed of a 2-DOF planar robot, force sensor, and a 2-DOF passive arm support.

$L = 1e{-}3 \cdot \mathbb{I}_3$, initial system parameter estimate $\hat{\theta}(0) = [0, 0, 0]^{\mathsf{T}}$, $p = 1e{-}3$, $\beta = \frac{\pi}{6}$ rad, $\sigma = \frac{\pi}{2}$ rad, $w_s = 0.01$, and $h_t = 0.01$ m. A straight desired trajectory with zero initial and final velocities and accelerations, from $[0.4\ 0.3]$ m to $[-0.1\ 0.3]$ m, between time $t = 0$ s and $t = 50$ s, was set as

$$\begin{bmatrix} x_{\mathrm{des},1}(t) \\ x_{\mathrm{des},2}(t) \end{bmatrix} = \begin{bmatrix} 0.4 - 4e{-}5\Delta t^3 + 1.2e{-}6\Delta t^4 - 9.6e{-}9\Delta t^5 \\ 0.3 \end{bmatrix}$$

with the fixed trajectory reference $x_i = [0\ 0]^{\mathsf{T}}$ and $\Delta t = t - t_0$.

Three sets of tests were conducted. Test I investigated the assistive performance of the controller by its trajectory tracking ability starting within the R-DR when human region radius was set as $a_h = 0$ m. Outer radii of increasing and decreasing R-DRs were computed as $a_i = 0.0191$ m and $a_r = 0.0494$ m. Test II investigated the rehabilitative performance by human-dominant region following and human action encouragement in human region. The human-dominant region radius was set as $a_h = 0.05$ m, which meant $a_i = 0.0525$ m and $a_r \approx 0.0703$ m accordingly. The system started within human-dominant region and was intentionally pushed by the subject toward $-x_2$ direction (sideways) in this test. Trajectories, positional errors, and velocities of Test I and II are shown in Figs. 8 and 9, respectively. The root-mean-squared region and velocity errors are given in Table I. In both cases, the actual trajectories tracked the desired trajectory (I) or human-dominant region (II) closely. Region and
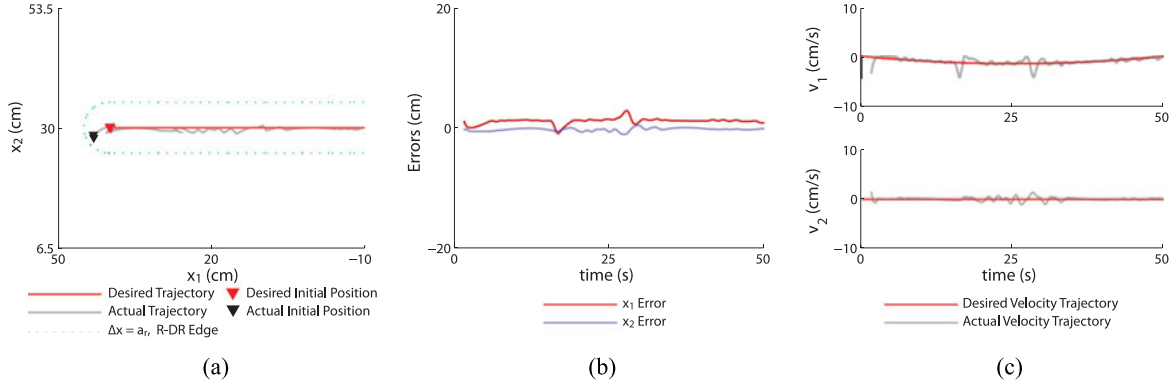
Fig. 8. Experimental results for assistive performance test, i.e., $a_h = 0$. (a) Desired and actual trajectories in space. (b) Position tracking errors of both x and y directions in time domain. (c) Desired and actual velocities of both directions in time domain, in which v_1 denotes velocity on x_1 axis and v_2 is velocity on x_2 axis.
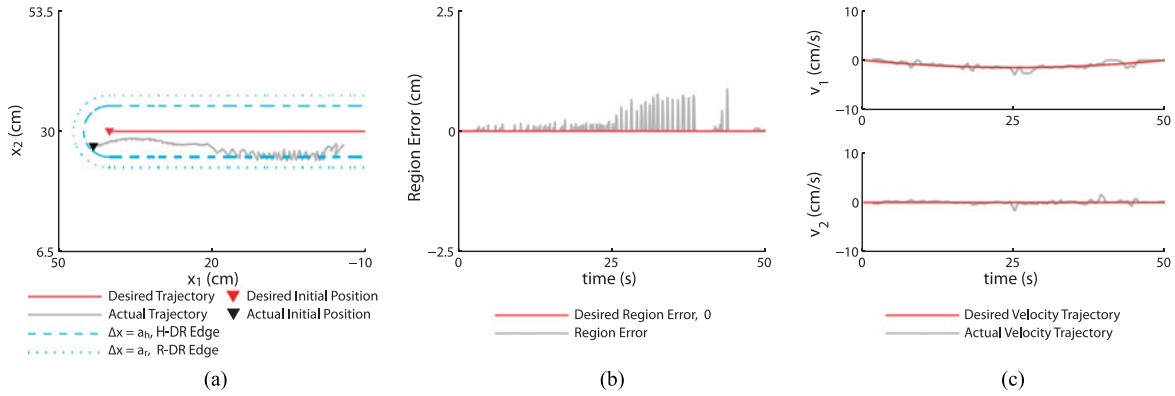

Fig. 9. Experimental results for rehabilitative performance test with $a_h = 0.05$ m. (a) Desired and actual trajectories in space. (b) Region errors $e_r = \max(||\Delta x|| - a_h, 0)$ versus time. (c) Desired and actual velocities in time domain.

TABLE I
RMS VALUES FOR REGION ERROR, $e_r = \max(||\Delta x|| - a_h, 0)$, AND VELOCITY TRACKING ERROR, WHICH IS DEFINED AS $e_v = ||\dot{x} - \dot{x}_{\mathrm{des}}||$, IN 2-D EXPERIMENTS

	Test I	Test II
RMS e_r	0.01305 m	0.00147 m
RMS e_v	0.0102 m/s	0.0035 m/s

velocity tracking errors were both smaller in Test II compared with I.

Test III demonstrated the safety-stop capability of the controller using $a_h = 0.05$ m. The end-effector started in human-dominant region and was intentionally pushed into the safety-stop region by a large human force. The system stopped in the safety-stop region after forced into this area (see Fig 10).

High oscillations and errors in the data were due to slow response and high frictions of the testbed, which had a control delay of 0.05 s. Part of the velocity errors also came from the differentiation of position data. Tests I and II demonstrated the system capabilities of trajectory-tracking and region-recovery in assistive and rehabilitative modes and showed that the system possessed the ability to interact with the human in a stable manner. Test III confirmed the safety-stop capability of the
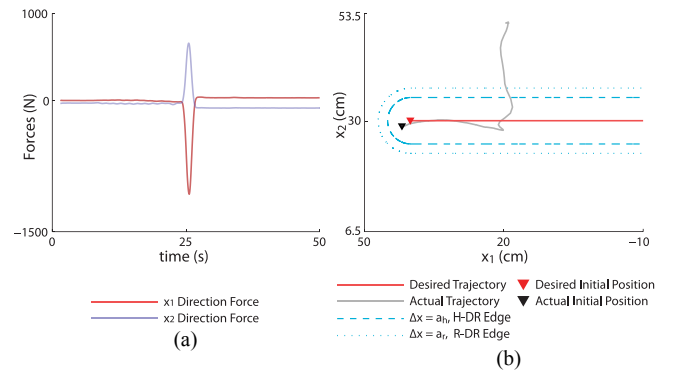

Fig. 10. Experimental results for safety-stop performance test with $a_h = 0.05$ m and $a_r = 0.0703$ m. (a) The force spike applied at the handle by the subject in time domain. (b) The desired and actual spatial trajectories.

controller. In Test I, velocity errors were relatively larger since the system operated in R-DR, where velocity tracking was less dominant. In contrast, due to the existence of human-dominant region and large amount of time in it, where velocity control was dominant, Test II had smaller velocity errors. System performance is expected to improve using a faster hardware with less sensory and actuation delays.

In actual rehabilitation, one therapy does not fit the conditions of different patients at different stages. The system should thus provide flexibility for therapists to adjust and fine tune. The proposed controller, while possessing all the properties described, allows parameter adjustment. When implementing this controller on a specific device, the parameter tuning process should start with the therapist's assessment of the patient's conditions. If the patient is at early stage of the therapy and has minimal motion control, the radius of human-dominant region a_h should be set very small to ensure maximum robot assistance. Then, along the training process, with the improvement of patient's motion control ability, a_h should be progressively set larger to encourage patient's active movements. With a_h fixed, the size of R-DR, denoted by a_r, should be determined to avoid injuries from large input torque or excessive human joint movements. Similarly, in interaction-related controller, β and σ should be made smaller when the patient has less motion control and then adjusted to a larger value when the patient improves. Based on the region sizes determined by the therapist above, location of the end-effector and direction of the human interaction then define the "correct" and "incorrect" movements. For example, an end-effector position in human-dominant region is considered correct and deviation from it is considered incorrect; an interaction force directed to $-s_x$ is correct, while a force opposite to $-s_x$ is incorrect. These clinically chosen parameters are then fed into the controller system to be realized by our control framework.

Other parameters k_1, K_s, L, α, h_t, w_s, are control performance related that should be tuned by control engineers before the start-up of the device and then fixed or limited to a small fine-tuning zone for the clinical training. Choice of k_1 should be balanced between maximum human bearable torque and the region tracking performance. Then, K_s and α are fine tuned together to achieve desired region-tracking, velocity-tracking, and steady-state error performance of the controller. Short region restoration rise time can be achieved by tuning k_1 up and better velocity tracking can be done by tuning K_s up. Smaller steady-state error can be achieved by higher α. Finally, the parameter adaptation gain L should start with very small values and be tuned up when faster adaptation is desired.

The capabilities of adjustability, customizability, safety, and stability of the controller provide a dependable control platform for clinical upper-limb rehabilitative training using robotic systems. This controller is motion-dominant with the compensation of interaction-handling. Motion-dominant robot-assisted rehabilitation training is an intuitive imitation of traditional therapies, which is still used in a lot of upper-limb rehabilitative devices [6], [5], [27]. It has been shown to be an effective substitute for traditional therapist-based training [28] with comparable training results and reduced human labor intensity. Other alternative methods start to show promises in rehabilitation, for example, the manipulation of joint energy input [29], which is especially popular for lower limb applications [30] in stance phase of walking due to the high-power-density nature of human locomotion.

VI. Conclusion

In this paper, a controller infrastructure for upper-limb rehabilitative robotics used in reaching and tracking training, which realizes three control modes, namely human-dominant mode, robot-dominant mode, and safety-stop mode, has been developed. With the employment of position-dependent stiffness and position-dependent desired trajectory, the proposed controller possesses the capability of automatic smooth transition between different operation modes to realize "assist-as-needed" strategy. By this controller, the passivity of upper-limb rehabilitative robotic system has been established, the stability of the closed-loop system has also been solved with system nonlinearities, uncertainties, and varying human–robot interactions; besides, the conflicts between the movements of robot and human user have been reduced by the proposed controller in a stable manner. With this controller, the human–robot interactive rehabilitative system moves mostly inside human-dominant region to ensure human exercise of proper amount and will be pulled back if entering R-DR. Built-in safety-stop functionality is realized and triggered in case of over-sized position errors to avoid damage to human limbs. While guaranteeing all the properties described, the proposed controller allows parameter adjustment, which provides the therapists with the freedom to design patient-specific training processes. Computer simulation and pilot tests on hardware have illustrated the performances of the aforementioned capabilities of the proposed controller.

Although this paper focuses on rehabilitation robotics, the proposed controller with the safety-stop scheme can be applied to robotic devices that involve physical human–robot interaction to ensure safety.

References

[1] S. Freud, "Project for a scientific psychology," in *Proc. The standard edition of the complete psychological works of Sigmund Freud*, London: Hogarth Press, 1953, vol. 1, pp. 283–397.

[2] C. Shatz, "The developing brain," *Sci. Amer.*, vol. 267, pp. 60–67, 1992.

[3] M. Hallett, "Plasticity in the human motor system," *Neuroscientist*, vol. 5, pp. 324–332, Sep. 1999.

[4] W. M. Jenkins and M. M. Merzenich, "Reorganization of neurocortical representations after brain injury: A neurophysiological model of the bases of recovery from stroke," *Progress Brain Res.*, vol. 71, pp. 249–266, 1987.

[5] H. I. Krebs, N. Hogan, M. L. Aisen, and B. T. Volpe, "Robot-aided neurorehabilitation," *IEEE Trans. Rehabil. Eng.*, vol. 6, pp. 75–87, Mar. 1998.

[6] N. Hogan, H. I. Krebs, J. Charnnarong, P. Srikrishna, and A. Sharon, "Mit-manus: A workstation for manual therapy and training," in *Proc. Int. Workshop Robot Human Commun.*, Sep. 1992, pp. 161–165.

[7] M. Takegaki and S. Arimoto, "A new feedback method for dynamic control of manipulators," *J. Dynam. Syst., Meas. Control*, vol. 103, pp. 119–125, 1981.

[8] J. J. E. Slotine and W. Li, "On the adaptive control of robot manupulators," *Int. J. Robot. Res.*, vol. 6, pp. 45–59, 1987.

[9] S. Arimoto, *Control Theory of Non-linear Mechanical Systems: A Passivity-based and Circuit-theoretic Approach*. London, U.K.: Oxford Univ. Press, Dec. 1996.

[10] C. C. Cheah, M. Hirano, S. Kawamura, and S. Arimoto, "Approximate jacobian control for robots with uncertain kinematics and dynamics," *IEEE Trans. Robot. Autom.*, vol. 19, pp. 692–702, Aug. 2003.

[11] H. Kazerooni, J.-L. Racine, L. Huang, and R. Steger, "On the control of the berkeley lower extremity exoskeleton (bleex)," in *Proc. IEEE Int. Conf. Robot. Autom.*, Barcelona, Spain, Apr. 2005, pp. 4353–4360.

[12] L. Marchal-Crespo and D. J. Reinkensmeyer, "Review of control strategies for robotic movement training after neurologic injury," *J. NeuroEng. Rehabil.*, vol. 6, Jun. 2009. DOI: 10.1186/1743-0003-6-20

[13] N. Hogan, "Impedance control: An approach to manipulation: Part I – Theory," *ASME J. Dynam. Syst., Meas. Control*, vol. 107, pp. 1–24, Mar. 1985.

[14] N. Hogan and S. P. Buerger, "Impedance and interaction control," in *Robotics and Automation Handbook*. New York, NY, USA: CRC Press, 2005, pp. 1901–1924.

[15] J. A. Saglia, N. G. Tsagarakis, J. S. Dai, and D. G. Caldwell, "Control strategies for ankle rehabilitation using a high performance ankle exerciser," in *Proc. IEEE Int. Conf. Robot. Autom.*, May 2010, pp. 2221–2227.

[16] E. D. Fasse and N. Hogan, "Control of physical contact and dynamic interaction," in *Proc. 7th Int. Symp. Robot. Res.*, Munich, Germany, 1996, pp. 28–38.

[17] T. Nef, M. Mihelj, and R. Riener, "Armin: A robot for patient-cooperative arm therapy," *Med. Biol. Eng. Comput.*, vol. 45, pp. 887–900, 2007.

[18] S. K. Banala, S. K. Agrawal, and J. P. Scholz, "Active leg exoskeleton (alex) for gait rehabilitation of motor-impaired patients," in *Proc. IEEE 10th Int. Conf. Rehabil. Robot.*, 2007, pp. 401–407.

[19] L. L. Cai, A. J. Fong, C. K. Otoshi, Y. Liang, J. W. Burdick, R. R. Roy, and V. R. Edgerton, "Implications of assist-as-needed robotic step training after a complete spinal cord injury on intrinsic strategies of motor learning," *J. Neurosci.*, vol. 26, pp. 10 654–10 658, 2006.

[20] N. Vitiello, T. Lenzi, S. Roccella, S. M. M. D. Rossi, E. Cattin, F. Vecchi, and M. C. Carrozza, "Neuroexos: A powered elbow exoskeleton for physical rehabilitation," *IEEE Trans. Robot.*, vol. 29, pp. 220–235, Feb. 2013.

[21] G. A. Ollinger, J. Colgate, M. A. Peshkin, and A. Goswami, "Inertia compensation control of a one-degree-of-freedom exoskeleton for lower-limb assistance: Initial experiments," *IEEE Trans. Neural Syst. Rehabil. Eng.*, vol. 20, pp. 68–77, Jan. 2012.

[22] S. Haddadin, A. Albu-Schffer, and G. Hirzinger, "Safety analysis for a human-friendly manipulator," *Int. J. Soc. Robot.*, vol. 2, pp. 235–252, 2010.

[23] R. Riener, L. Lunenburger, S. Jezernik, J. M. Anderschitz, G. Colombo, and V. Dietz, "Patient-cooperative strategies for robot-aided treadmill training: First experimental results," *IEEE Trans. Neural Syst. Rehabil. Eng.*, vol. 13, pp. 380–394, Sep. 2005.

[24] J. Zhang, C. C. Cheah, and S. H. Collins, "Stable human-robot interaction control for upper-limb rehabilitation robotics," in *Proc. IEEE Int. Conf. Robot. Autom.*, Karlsruhe, Germany, May 2013, pp. 2201–2206.

[25] J.-J. E. Slotine and W. Li, *Applied Nonlinear Control*. Englewood Cliffs, NJ, USA: Prentice-Hall, 1991.

[26] S. Hanneton, A. Berthoz, J. Droulez, and J. J. E. Slotine, "Does the brain use sliding variables for the control of movements?" *Biol. Cybern.*, vol. 77, pp. 381–393, 1997.

[27] M. A. Finley, S. E. Fasoli, L. Dipietro, J. Ohlhoff, L. MacClellan, C. Meister, J. Whitall, R. Macko, C. T. Bever, H. I. Krebs, and N. Hogan, "Short-duration robotic therapy in stroke patients with severe upper-limb motor impairment," *J. Rehabil. Res. Dev.*, vol. 42, pp. 683–692, 2005.

[28] S. Masiero, M. Armani, and G. Rosati, "Upper-limb robot-assisted therapy in rehabilitation of acute stroke patients: Focused review and results of new randomized controlled trial," *J. Rehabil. Res. Dev.*, vol. 48, pp. 355–366, 2011.

[29] A. H. A. Stienen, E. E. G. Hekman, H. ter Braak, A. M. M. Aalsma, F. C. T. van der Helm, and H. van der Kooij, "Design of a rotational hydroelastic actuator for a powered exoskeleton for upper limb rehabilitation," *IEEE Trans. Biomed. Eng.*, vol. 57, pp. 728–735, Mar. 2010.

[30] G. S. Sawicki and D. P. Ferris, "Powered ankle exoskeletons reveal the metabolic cost of plantar flexor mechanical work during walking with longer steps at constant step frequency," *J. Exp. Biol.*, vol. 212, pp. 21–31, Jan. 2009.

Juanjuan Zhang was born in Shandong, China. She received the B.E. degree with a major in electrical and electronic engineering and a minor in computing from Nanyang Technological University, Singapore, in 2007 with first class honors. She is currently working toward the dual-Ph.D. degree from the Department of Mechanical Engineering, Carnegie Mellon University, Pittsburgh, PA, USA, and the School of Electrical and Electronic Engineering, Nanyang Technological University, Singapore.

Her research interests include adaptive control, rehabilitation robots, and bipedal robots.

Chien Chern Cheah was born in Singapore. He received the B.E. degree in electrical engineering from National University of Singapore, Singapore, in 1990, and the M.E. and Ph.D. degrees in electrical engineering, from Nanyang Technological University, Singapore, in 1993 and 1996, respectively.

He is an Associate Professor with the School of Electrical and Electronic Engineering, Nanyang Technological University. He is an Associate Editor for Automatica.